

Investigation of elastic weakening in limestone and sandstone samples from moisture adsorption

L. Pimienta, J. Fortin and Y. Guéguen

Laboratoire de Géologie, Ecole Normale Supérieure, Paris F-75005, France. E-mail: pimienta@geologie.ens.fr

Accepted 2014 July 2. Received 2014 June 30; in original form 2014 February 3

SUMMARY

Elastic and mechanical weakening from water saturation are widely known to occur in sedimentary rocks, and particularly in carbonate rocks. To improve our understanding of the physics underlying this phenomenon, ultrasonic ($f \sim 0.5$ MHz) elastic properties are measured on a large suite of clean limestones and sandstones at very low saturations from relative humidity (RH) variations at ambient conditions. Measurements clearly highlight an elastic weakening (i.e. decrease in elastic wave velocity) from moisture adsorption. P - and S -wave velocities are similarly affected by adsorption, but in a different way for limestones and sandstone samples. While the elastic properties of limestone samples show almost no RH dependence, a large weakening is observed for samples of Fontainebleau sandstone that increases with the samples' porosity. The main elastic weakening effect is likely to result from adsorption of fluid at grain contacts. It thus affects particularly granular rocks such as sandstones while well-cemented limestones are not affected. The granular model from Murphy *et al.*, accounting for surface energy effects, proves to be appropriate. Applying this model, it is shown that (i) P - and S -wave velocities have the same dependence on surface energy, which is consistent with the measurements and (ii) surface energy values obtained from the ultrasonic data using this model correlate with RH, and are consistent with the expected value for quartz crystals at vapour pressure. Yet, porosity, which relates to degree of cementation in the particular case of Fontainebleau sandstone, appears to be an additional parameter. A modified model is thus derived using the cementation model from Digby, accounting for a bonding radius at grain contact. It proves to apply well to the measured data. The fundamental difference between limestones' and sandstones' dependence to RH appears to be related to a microstructural difference. Saturation variations from RH increase depend on specific surface area, which is particularly low in Fontainebleau sandstones and large in microporous limestones. However elastic weakening from RH is more important in sandstones owing to their granular microstructure.

Key words: Microstructure; Elasticity and anelasticity; Mechanics, theory, and modelling.

1 INTRODUCTION

Sedimentary rocks are porous media that present, under fluid saturation, a large surface area where mineral and fluid are in contact. Depending on the pores' content and shape, rock–fluid interaction may be important enough to directly affect the rock physical properties. This effect has often been evasively referred to as 'shear weakening' or 'Rebhinder effect'. While this effect has been observed for sandstones' mechanical strength (e.g. Kirby 1984; Baud *et al.* 2000; Klein *et al.* 2001; Fortin *et al.* 2007), a few measurements of elastic properties (e.g. Winkler & Murphy 1995) also reported it. In recent years, more emphasis was given to the microstructurally complex carbonates (e.g. Verwer *et al.* 2008). These rocks have been shown to be very sensitive to the saturating fluid,

and elastic properties, such as the shear modulus, appear to decrease upon water saturation (e.g. Assefa *et al.* 2003; Baechle *et al.* 2005; Adam *et al.* 2006; Verwer *et al.* 2008; Fabricius *et al.* 2010). Such behaviour is not consistent with established theories that consider the shear modulus as unaffected by fluid (Gassmann 1951). This elastic weakening phenomenon is reversible and disappears under drying (Baechle *et al.* 2005), and thus seems related to adsorption. This weakening from adsorption appears to be more important in limestone than in sandstone samples (e.g. Baechle *et al.* 2005).

In order to understand the elastic weakening linked to adsorption, low saturations (i.e. corresponding to adsorbed volumes) are investigated. Low saturation is attained through varying the partial pressure of the atmosphere surrounding the sample (e.g. Clark *et al.* 1980; Tittmann *et al.* 1980). Effects of moisture and adsorption

were in particular experimentally investigated to understand the fundamental difference between attenuations of lunar and terrestrial rocks (e.g. Tittmann & Housley 1973; Tittmann 1977, 1978), and to study the induced elastic weakening (e.g. Clark *et al.* 1980) and attenuation (e.g. Pandit & King 1979; Clark *et al.* 1980; Murphy 1982, 1984) at seismic frequencies. Theories have been proposed to explain these observations (e.g. Johnson *et al.* 1971; Murphy *et al.* 1984; Tutuncu & Sharma 1992; Chelidze *et al.* 1996). In particular, based on the analysis of Johnson *et al.* (1971), Murphy *et al.* (1984) and Tutuncu & Sharma (1992) developed models to predict elasticity and/or attenuation variations as a function of moisture adsorption. Yet, velocities (Clark *et al.* 1980) and attenuations (e.g. Tittmann *et al.* 1980) were measured at seismic ($f \sim 1$ kHz) frequencies only and very few clean sandstone and limestone samples were studied.

In this study, sensitivity of sandstones' and carbonates' elastic properties to adsorption are compared at room T–P. Water saturations and ultrasonic ($f \sim 0.5$ MHz) wave velocities are measured under controlled relative humidity (RH). To understand the underlying physics, the micromechanical model of Murphy *et al.* (1984) is introduced that links effective elasticity to surface energy (Johnson *et al.* 1971). Finally, cementation is accounted for using the model of Digby (1981) to understand the less porous sandstones.

2 EXPERIMENTAL APPROACH AND SAMPLES STUDIED

2.1 Samples studied

This study investigates the role of adsorption on elastic properties of clean (i.e. calcite- and quartz-pure, respectively) limestones and sandstones of varying porosity. A suite of 11 limestone and nine sandstone samples, covering a wide range in porosity for both sedimentary rocks, were selected. The samples' main petrophysical features are presented in Table 1, that reports measured porosities (ϕ), along with permeabilities (κ) and pore entry diameters (d) found in the literature. The total pore volume V_{pore} (leading to ϕ) is obtained from the dry density of the rock samples and the quartz/calcite crystal densities. As the samples are clean (i.e. quartz- or calcite-pure) rocks, this approach is preferred over any other porosity measuring method.

2.1.1 Fontainebleau sandstone samples

Fontainebleau sandstone is a well-known reference rock. Many experimental investigations have been carried out on this rock (e.g. Song & Renner 2008; Gomez *et al.* 2010; Duda & Renner 2013). It exhibits homogeneous and isotropic properties at the sample scale (e.g. Sulem & Ouffroukh 2006). Both framework grains and cement are pure quartz, making up a clean sandstone of about 99.9 per cent quartz (e.g. Bourbie & Zinszner 1985). This aeolian rock is well sorted, with a relatively constant grain radius (r) of about $r \sim 100$ μm .

Depending on the amount of quartz cementing, its porosity ranges from about $\phi \sim 2$ per cent for highly cemented samples to about $\phi \sim 25$ per cent for less cemented samples (Bourbie & Zinszner 1985). The variable amount of quartz cement originates from a variation in the silica super-saturated water-table (e.g. Sulem & Ouffroukh 2006). As a consequence, pore-entry diameters (d) decrease with porosity (e.g. Song & Renner 2008) from $d \sim 20$ μm to about $d \sim 5$ μm , leading to variations in permeability of about 4–5 orders of magnitude (Bourbie & Zinszner 1985).

In this study, Fontainebleau samples with a porosity ranging from about $\phi \sim 2$ per cent up to about $\phi \sim 20$ per cent are investigated.

2.1.2 Limestones

Apart from Indiana limestone, the limestone samples chosen come from French quarries (e.g. Vincent *et al.* 2011). They vary in porosity, morphology (e.g. grains and pores size) and sedimentary history (e.g. micritic versus oolitic limestones). All samples are considered as clean limestones, and all of them exhibit a double porosity.

Tavel limestone is a relatively homogeneous micritic limestone (Vajdova *et al.* 2004) made up of a microcrystalline matrix relatively well cemented with an average grain diameter of ~ 5 μm . Its porosity is $\phi \sim 17$ per cent. It is characterized by a bimodal pore-size distribution of few macropores (i.e. $d \sim 100$ μm), and mainly submicron (i.e. $d \sim 0.1$ μm) pores (Vajdova *et al.* 2010). Indiana limestone is an oolitic limestone with fossils of about ~ 300 μm diameter cemented by fine-grained calcite (Vajdova *et al.* 2004). Estaillade and Fontvieille limestones originate from Gard quarries from southeast France. Both are calcite-pure bioclastic micritic rocks of large porosities (i.e. $\phi \sim 28.4$ per cent and $\phi \sim 23.6$ per cent, respectively). Estaillade limestone exhibits a bimodal pore size distribution made up of intergranular macro-pores of about $d \sim 19$ μm and intra-granular micropores of $d \sim 0.39$ μm (Youssef *et al.* 2008).

The other limestones are from the Oolite Blanche carbonate formation of Paris Basin. Euville limestone is an oolitic limestone with a bimodal porosity ($\phi \sim 22$ per cent) mainly composed of inter- ($d < 80$ μm) and intra- ($d < 1.5$ μm) oolite pores (Eslami *et al.* 2010). Lavoux and Chauvigny limestones originate from the Dogger formation. Lavoux is an oolitic limestone (Le Guen *et al.* 2007; Vincent *et al.* 2011) as for one of the Chauvigny samples (Fortin *et al.* 2009; Vincent *et al.* 2011). The other Chauvigny sample is a fine-grained loosely cemented micritic rock. Lavoux sample has a porosity of about $\phi \sim 22$ per cent, and the oolitic and micritic Chauvigny samples have porosities of about $\phi \sim 16$ and ~ 34 per cent, respectively. All three samples show microporosity in the range of $d \sim 0.1$ – 1 μm , and a macroporosity of about $d \sim 10$ – 100 μm (Youssef *et al.* 2008). Anstrude, Raviere and Massangis limestones are characterized as oolitic limestones, and have a double porosity with very similar pore entry diameters of about $d \sim 0.1$ – 0.6 μm for the microporosity (Casteleyn *et al.* 2010). While Anstrude and Raviere samples have similar total porosity of about $\phi \sim 19$ per cent, Massangis limestone has a lower porosity ($\phi \sim 6$ per cent) that probably originates from differing degrees of cementing during burial.

The 20 samples in Table 1 are ranked from low porosity to high porosity values. The values of permeability and pore-entry diameter correlate to porosity for the Fontainebleau sandstone samples only.

2.2 Experimental set-up

In order to measure small quantities of water saturation ($S_w < 2$ per cent), we impose varying RH in the atmosphere surrounding the rock sample. This experiment aims at investigating (i) the amount of water adsorbed; and (ii) the effects of adsorption on elastic properties. An experimental protocol is thus devised to study the evolution of rocks' elastic properties with adsorption.

2.2.1 RH control

The atmosphere's RH is defined as the ratio between the water pressure $P_{\text{H}_2\text{O}}$ and the pressure of saturating vapour P . Saturating

Table 1. Properties of the tested samples. Porosities (ϕ) as measured in this work. Approximate permeability (κ) and pore entry diameter (d) are reported from previous studies on the different samples.

Samples	Classification	ϕ (per cent)	κ (m^2)	d (μm)	References
Massangis	Oolite	6.1	1×10^{-16}	0.1–0.8 and 100	Casteleyn <i>et al.</i> (2010)
Indiana	Oolite	12.4	2×10^{-15}	0.04–1 and 100	Vajdova <i>et al.</i> (2004, 2010)
Euville	Oolite	15.9	4×10^{-15}	0.1 and 1–80	Eslami <i>et al.</i> (2010)
Chauvigny oolite	Oolite	16.3	–	0.1–2 and 10–50	Vincent <i>et al.</i> (2011)
Tavel	Micrite	17.2	1×10^{-17}	0.02–0.3 and 100	Vajdova <i>et al.</i> (2004)
Anstrude	Oolite	19.5	4×10^{-16}	0.3 and 100	Casteleyn <i>et al.</i> (2010)
Raviere	Oolite	19.7	2×10^{-16}	0.4 and 100	Casteleyn <i>et al.</i> (2010)
Lavoux	Oolite	22.4	1×10^{-14}	0.84 and 20	Le Guen <i>et al.</i> (2007)
Fontvieille	Micrite	23.6	–	–	–
Estaiillades	Micrite	28.4	2×10^{-13}	0.39 and 19	Le Guen <i>et al.</i> (2007)
Chauvigny micrite	Micrite	34.4	–	0.2–3 and 200	This work
Fontainebleau (FoSp2a)	Granular	2.6	1×10^{-17}	1–10	Bourbie & Zinszner (1985)
Fontainebleau (FoSp2b)	Granular	2.2	1×10^{-17}	1–10	Bourbie & Zinszner (1985)
Fontainebleau (FoSp4)	Granular	4.7	1×10^{-15}	1–10	Bourbie & Zinszner (1985)
Fontainebleau (FoSp7)	Granular	7.2	1×10^{-14}	1–10	Bourbie & Zinszner (1985)
Fontainebleau (FoSp9)	Granular	9.0	1×10^{-13}	10	Bourbie & Zinszner (1985)
Fontainebleau (FoSp16a)	Granular	16.0	1×10^{-12}	10–20	Bourbie & Zinszner (1985)
Fontainebleau (FoSp16b)	Granular	16.7	1×10^{-12}	10–20	Bourbie & Zinszner (1985)
Fontainebleau (FoSp18a)	Granular	18.2	5×10^{-12}	10–20	Bourbie & Zinszner (1985)
Fontainebleau (FoSp18b)	Granular	18.9	5×10^{-12}	10–20	Bourbie & Zinszner (1985)

vapour pressure depends on different factors such as temperature, which is continuously monitored during experiment and is about $T = 20 \pm 2^\circ\text{C}$. For a given RH, equilibrium between vapour and liquid water leads to adsorption of small amounts of water on the rock pores surfaces. Adsorption equilibrium on a mineral surface from RH is usually reached within a few minutes. Weight measurements showed that final saturation of the rock (i.e. mineral aggregate) is reached in less than 1 hr after RH stabilization.

The prepared sample is introduced in the hermetically closed glass chamber using a system allowing for direct measurement of elastic wave velocities under controlled atmosphere (Fig. 1). In this study, RH is controlled by the presence of different salts in a closed chamber (e.g. Greenspan 1977). For a given temperature, each salt (or salt solution) is chosen as leading to a calibrated RH (Fig. 1). To measure precisely the RH, a Thermo-Hygrometer ‘Testo

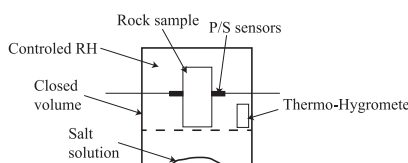
610’, accurate to the 1st decimal, is introduced in the volume. It also allows for a constrained tracking of the RH equilibrium and stabilization, with an accuracy of ~ 0.1 per cent.

In this study, the sought properties were measured after 2 hr of RH stabilization, and after 4 hr in the extreme case of maximum RH (i.e. ~ 95 per cent). RH and elastic wave velocities are measured simultaneously directly in the chamber, and mass is measured directly when opening the chamber.

2.2.2 *P*- and *S*-waves velocities

Cylindrical rock samples of 80 mm length and 40 mm diameter are used in the study. Before experiments, samples are dried in an oven filled with anhydrous salts at $T \sim 70^\circ\text{C}$, and then weighted to obtain the total pore volume V_{pore} . Two couples of *P*- and *S*-wave piezoelectric transducers of $f \sim 0.5$ MHz central frequency are directly glued on the sample (Fig. 1). *P*- and *S*-sensors are opposed as to measure ultrasonic wave propagation across the samples’ diameter. In this set-up, the transducers are glued to the samples ‘once and for all’, that is they remain on the samples throughout the RH variations, giving constant travel paths and contact conditions. The sensors’ weight is considered to be independent of the RH so that the sample’s water saturation can be traced from the weight difference. The piezoelectric sensors are directly related to a standard generator sending a square pulse of $f \sim 0.5$ MHz central frequency, and an analogical oscilloscope linked to the Insite ASC Ltd data acquisition software (e.g. Ougier-Simonin *et al.* 2011).

Absolute *P*- and *S*-wave velocities under dry conditions (i.e. lowest RH of about ~ 5 per cent) are hand-picked. The evolution of the elastic velocities with RH is then obtained by a cross-correlation with this reference state at lowest RH. Measurements of absolute elastic wave velocities may have a low accuracy, owing to (i) the uncertainty in wave arrival and (ii) the sensors’ position and the



	Salt 1	Salt 2	Salt 3	Atmosphere	Salt 4	Salt 5
Salt name	Anhydrous	KCH_3CO_2	K_2CO_3		NaCl	K_2SO_4
Relative Humidity (RH)	$5 \pm 2\%$	$23 \pm 3\%$	$43 \pm 3\%$	$60 \pm 5\%$	$75 \pm 3\%$	$95 \pm 3\%$

Figure 1. Schematic view of the experimental set-up. The prepared sample is placed in the closed volume along with a salt solution that will affect RH. Elastic wave velocities are measured directly on the sample at ambient conditions after RH stabilization. Five different salts are used to change RH, each corresponding to a different RH value. For a given temperature, each salt (or salt solution) is chosen as leading to a calibrated RH (e.g. Greenspan 1977).

sensors-to-sample contact quality that vary from one sample to the other. As a consequence, uncertainty on P - and S -wave velocities' absolute measurement may be as high as about ~ 2 and ~ 5 per cent, respectively. However, P - and S -wave velocities' relative measurements, obtained from waveforms' cross-correlation, allow to discard these sources of uncertainty, leading to an accuracy of about ~ 0.1 per cent.

2.2.3 Water saturation

Mass variation is measured with an accuracy of $\Delta m \sim 0.01$ mg. Water saturation S_w is then deduced from pore volume (i.e. V_{pore}) and Δm using the relation:

$$S_w = \frac{\Delta m}{\rho_{\text{wat}} \cdot V_{\text{pore}}}, \quad (1)$$

with ρ_{wat} the water density. The measurement proves to be accurate to about ~ 2 per cent for most samples. Only in the case of Fontainebleau sandstones with the lowest porosity, the error in S_w goes up to about ~ 5 per cent.

3 EXPERIMENTAL RESULTS

The first aim is to study the differences between limestones and sandstones. Thus different symbols are used for both rock types in the various figures.

3.1 Elastic properties ($V_p - V_s$) at low RH

The samples' absolute P - and S -wave velocities measured under dry condition are reported (Fig. 2) as a function of their porosity. Overall, P waves (Fig. 2a) and S waves (Fig. 2b) show similar trends. Velocities decrease with increasing porosity. Yet, these trends appear to differ between rock types (i.e. Limestones versus Fontainebleau sandstone samples). While Fontainebleau samples exhibit large velocity variations with porosity, limestones samples show smaller variations.

Clear differences between oolite and micrite limestones dry elastic properties are not found. As a consequence, elastic properties of these two limestones families are undifferentiated in the following, and we focus only on the difference between limestones and sandstone samples.

3.2 Evolution of properties with RH

To fully investigate the effect of adsorption on elasticity, two main properties are measured: (i) water saturation; and (ii) normalized P - and S -wave velocities.

3.2.1 Water saturation

The evolution of the sample saturation is measured (Fig. 3) as a consequence of an increase in RH. Two important differences appear between rocks type. While limestones exhibit large variations in water saturation with RH, only very small increases are observed for the Fontainebleau samples. Limestones exhibit a large scattering from sample to sample, with values ranging from $S_w \sim 0.5$ per cent up to $S_w \sim 2.5$ per cent at maximum RH. On the reverse, Fontainebleau samples show a small scattering and a water saturation S_w remaining lower than ~ 0.5 per cent at highest RH. Saturation from adsorption thus proves to be larger in limestones than in Fontainebleau samples.

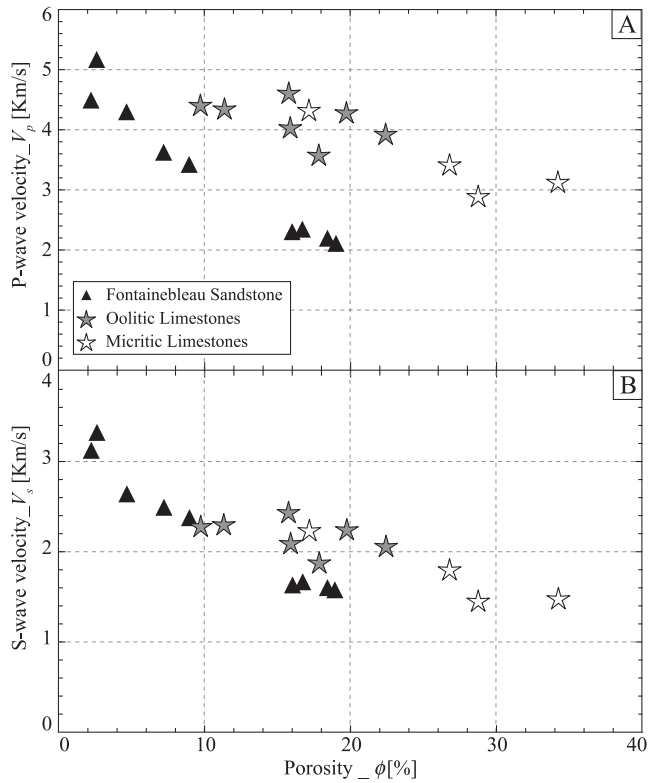


Figure 2. Measured dry P - and S -wave velocities at ambient conditions on the Limestones (stars) and Fontainebleau sandstone (triangles) samples. Limestones samples are grouped into oolitic (grey stars) and micritic (white stars).

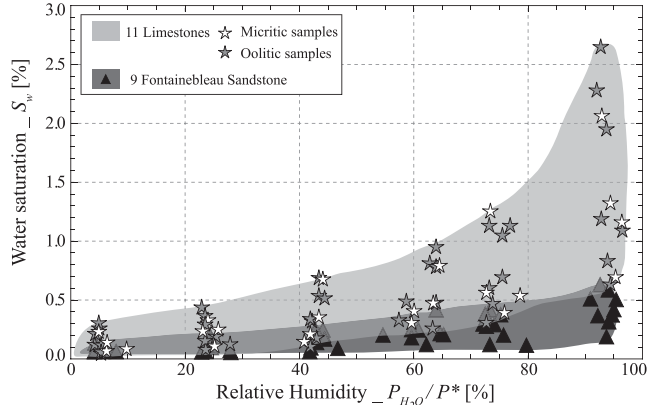


Figure 3. Measured water saturation variations with relative humidity on 11 limestones samples (grey surface and stars) and on nine Fontainebleau sandstones (triangles).

Again no clear difference is observed between oolites and micrites. Also, as the selected Fontainebleau samples have porosities ranging from $\phi \sim 2$ per cent to $\phi \sim 19$ per cent, it is clear that S_w depends very weakly on porosity in that case.

3.2.2 Normalized elastic wave velocities

An example of RH effect on P and S waveforms is introduced (Fig. 4) for the oolitic Chauvigny limestone and a Fontainebleau sandstone (FoSp16a). These samples have been selected for comparison because of their very similar porosity ($\phi \sim 16$ per cent). A clear difference between limestone and sandstone samples is observed

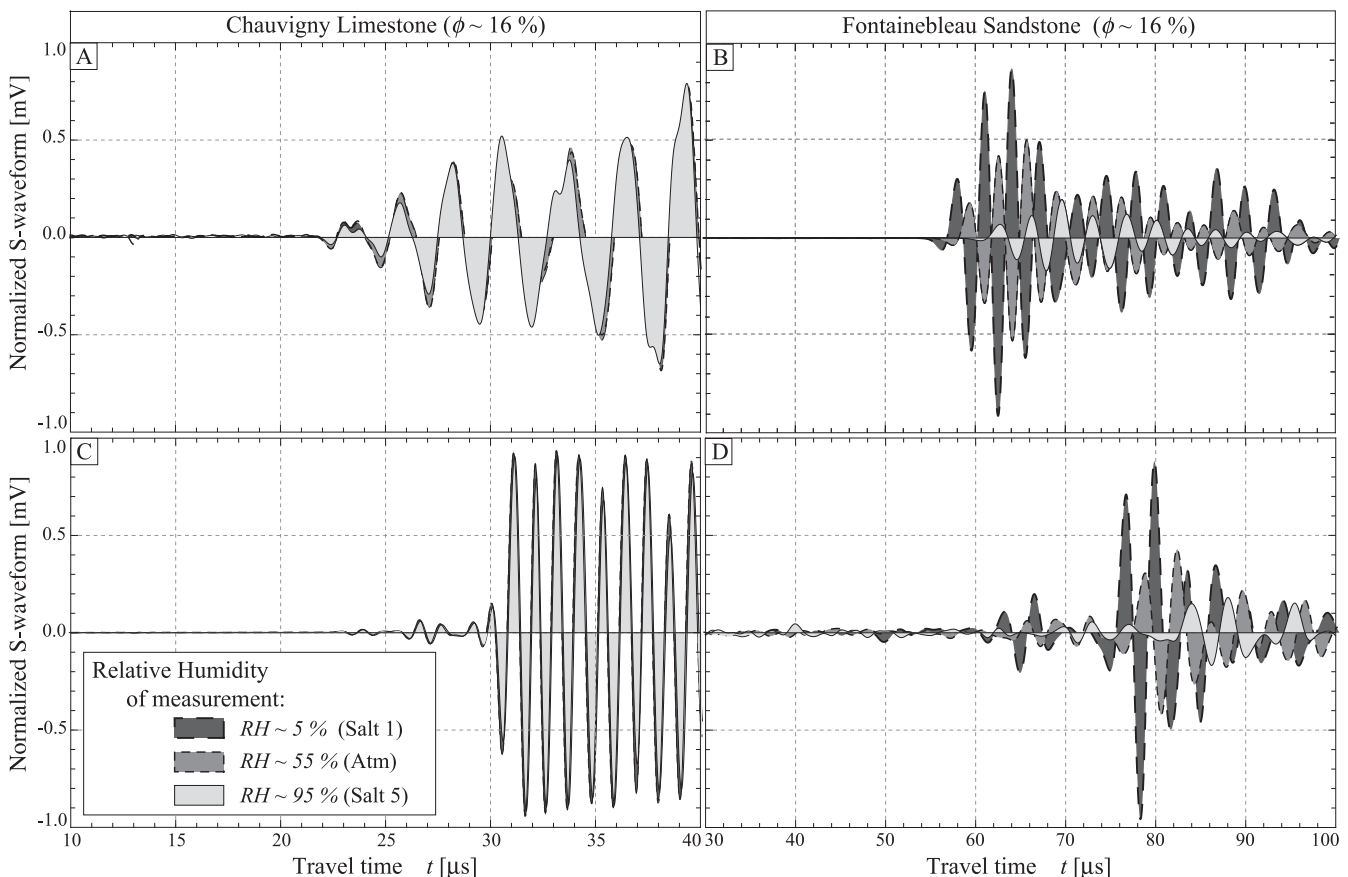


Figure 4. Normalized P - and S -waveforms measured at ambient conditions on a Chauvigny limestone sample (A and C) and a Fontainebleau sandstone sample (B and D) for three different Relative Humidities.

for both P (Figs 4a and 4b) and S (Figs 4c and 4d) waveforms. While waveforms measured on ChLo show no change with RH, large decrease in both arrival times and amplitudes is observed for FoSp16 with increasing RH. P - and S -wave velocities are directly inferred from the arrival times.

Variations of normalized P - and S -wave velocities for all samples are finally reported (Fig. 5) as a function of RH. While limestones velocities vary very slightly with RH (up to about ~ 0.5 per cent at maximum RH), some sandstone samples exhibit a large decrease (up to about ~ 25 per cent at maximum RH) with increasing RH.

Given that the variations for limestones are very small (i.e. ≤ 0.5 per cent), it is difficult to evidence any porosity or facies dependence. On the reverse, Fontainebleau sandstone samples show large variations as a function of RH. This dependence to RH correlates well to their porosities. Note that P wave (i.e. Fig. 5a) and S wave (i.e. Fig. 5b) have very similar dependencies on RH, and show the same order of magnitude of decrease at maximum RH.

An anticorrelation appears between saturation (Fig. 3) and elastic properties (Fig. 5) variations with RH. The limestones exhibit large saturation variations but almost no change in P and S waves with RH. On the reverse, the Fontainebleau samples exhibit lower saturation changes but show large P - and S -waves velocity variations.

4 INTERPRETATION OF ELASTIC WEAKENING USING EFFECTIVE MEDIUM THEORIES

As shown in Section 3, elastic velocities in Fontainebleau samples (Fig. 5) appear to depend on the moisture content, while such

relation is not observed for limestones. Furthermore, weakening in this quartz-pure sandstone increases with porosity. These measurements thus confirm that weakening from moisture does not originate from the presence of clay minerals (Clark *et al.* 1980), but from the rock microstructure (Murphy *et al.* 1984).

Effective medium models are relevant to analyse the reported results. Depending on the rock microstructure, two distinct approaches can be used. The first one consists in describing the pores as inclusions in a matrix. This approach holds particularly well in the case of rocks bearing isolated pores, or in the case of connected pores in a rock with strong grain boundaries. The second approach is more appropriate for a granular medium where stiffnesses at grain contact are the key element (e.g. Digby 1981). Following Murphy *et al.* (1984), this second approach is used below to investigate the measurements on the sandstone samples.

In particular, Murphy *et al.* (1984) developed an effective medium model that allows for adsorption at grain contacts. Adsorption modifies the frame moduli of a granular rock. This is consistent with the observations that RH effect appears mainly in the more porous and probably less cemented Fontainebleau sandstone samples.

4.1 Model from Murphy *et al.* (1984) applied to velocity data

The modelling approach from Murphy *et al.* (1984) relies on (i) the assumption that the rock frame moduli depend on the stiffness at the grain contact (e.g. Digby 1981), which in turn is a function of the surface energy at the contact between grains (Johnson *et al.* 1971) and (ii) a thermodynamic approach that relates surface energy to RH.

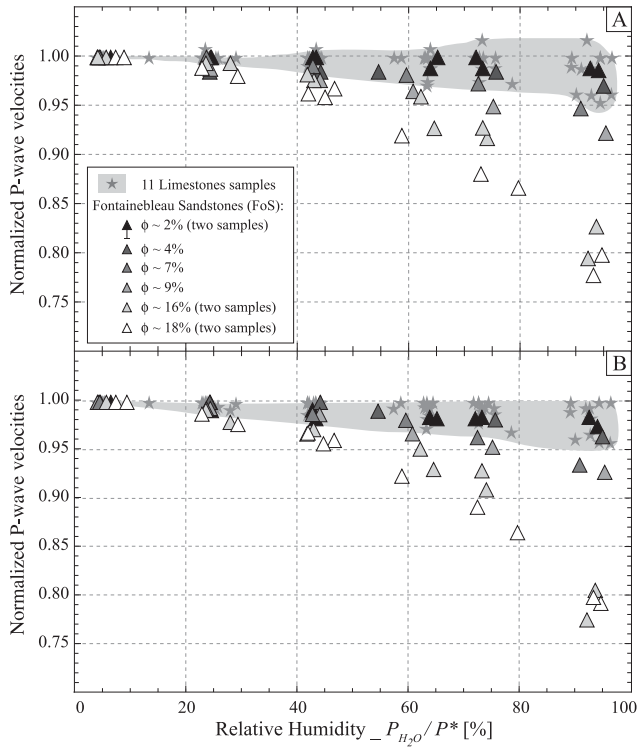


Figure 5. Normalized P - and S -wave velocity variations with relative humidity measured at ambient conditions on 11 limestones samples (grey surface and stars) and on nine Fontainebleau sandstone samples (triangles) of increasing porosities (filling in grey levels from black to white).

4.1.1 Model derivation

From energy considerations, Johnson *et al.* (1971) redefined the micromechanical model of Mindlin (1949). They showed that the contact radius a_1 at the interface also depends on surface forces (Fig. 6a), and thus slightly deviates from Hertz's contact radius a_0 . These surface forces are introduced through the surface energy γ at the interface such that:

$$a_1^3 = \frac{3(1 - \nu_m)r}{8G_m} \left[F + 6\gamma\pi r + \sqrt{12\gamma\pi rF + (6\gamma\pi r)^2} \right], \quad (2)$$

where F is the external load applied on the grains of radius r , G_m and ν_m are the shear modulus and Poisson ratio of the grain, and $\gamma = \gamma_0 - \Delta\gamma$ is the surface energy at a given state of adsorption (or RH) as a function of the dry surface energy of the crystal γ_0 . In the case of zero surface energy (i.e. $\gamma = 0$), one obtains the usual Hertz expression for contact radius $a_1 = a_0$. The γ -dependence predicted

by eq. (2) becomes negligible if $F \gg 6\pi\gamma r$. Since $F \sim Pr^2$, where P is the applied pressure, the effect is in theory observed only if $P \ll P_c = \frac{6\pi\gamma}{r}$, that is $P_c \sim 10$ MPa.

From this new contact radius a_1 , Johnson *et al.* (1971) showed that the normal (i.e. D_n) and tangential (i.e. D_t) stiffnesses from basic contact theory (Mindlin 1949) were affected by the surface energy γ at grain contact:

$$\begin{cases} D_n = \frac{2G_m a_1}{1 - \nu_m}, \\ D_t = \frac{4G_m a_1}{2 - \nu_m}, \end{cases} \quad (3)$$

where G_m and ν_m are the shear modulus and Poisson ratio of the mineral grain.

Finally, by combining eqs (2) and (3) (i.e. JKR model) with an homogenization approach (e.g. Wang & Nur 1992), Murphy *et al.* (1984) showed that the effective compressional (i.e. M_1) and shear (i.e. G_1) moduli of an aggregate (e.g. sandstones) were dependent on surface energy γ :

$$\begin{cases} M_1 = \rho \cdot V_p^2 = \frac{3(1 - \phi)\psi}{20\pi r} \left(D_n + \frac{2}{3} D_t \right), \\ G_1 = \rho \cdot V_s^2 = \frac{(1 - \phi)\psi}{20\pi r} \left(D_n + \frac{3}{2} D_t \right), \end{cases} \quad (4)$$

where ψ is the average number of contacts per grains (i.e. co-ordinance), and ϕ is the the sample porosity.

Normalizing M_1 (or G_1) to the dry reference state $M_1(\gamma_0) = M_{10}$ (or $G_1(\gamma_0) = G_{10}$), one discards parameters such as co-ordinance number ψ and the sample porosity ϕ . It is interesting to note that (i) normalization of either M or G leads to the same result; (ii) the remaining expression corresponds to the ratio of intermediate a_1 over reference a_{10} contact radii and (iii) the parameters at hand are constant in all Fontainebleau sandstone samples:

$$\frac{M_1}{M_{10}} = \frac{G_1}{G_{10}} = \frac{a_1}{a_{10}} = f(F, G_m, \nu_m, r, \gamma_0, \gamma). \quad (5)$$

The normalized P - and S -wave velocities (i.e. RV_p and RV_s) are directly obtained from the normalized compressional (i.e. M_1) and shear (i.e. G_1) moduli, respectively.

This final result is consistent with the present measurements of normalized V_p and V_s variations with RH that show the exact same trends (Fig. 5). Interestingly, compressional and shear modulus appear affected similarly by adsorption. By comparing (Fig. 7) the variations of RV_p relative to RV_s and eq. (5), the measurements clearly fall on the linear trend predicted using the model of Murphy *et al.* (1984).

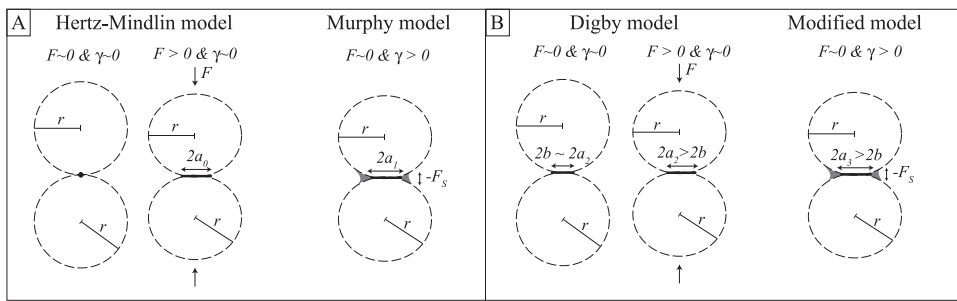


Figure 6. Schematic views of grain contact theories for (a) uncemented (i.e. no bonding radius b) and (b) cemented (i.e. existing bonding radius b) cases. The uncemented Hertz-Mindlin theory (a) is complemented by models from Johnson *et al.* (1971) and Murphy *et al.* (1984) for existing surface forces. The cemented theory from Digby (1981) is complemented by the present approach in case of surface forces.

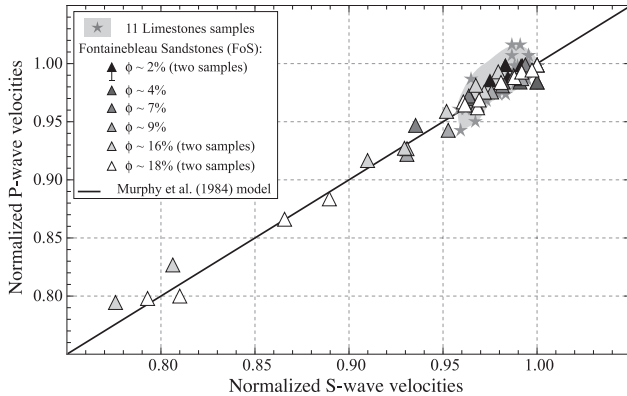


Figure 7. Relative variation of P -wave velocities as compared to S waves for varying relative humidities and values of surface energy. Measurements (symbols) are compared to the model prediction (black line) from Murphy *et al.* (1984).

4.1.2 Estimation of the surface energy

In the following, we focus on the data obtained on Fontainebleau samples as they show a large weakening with RH, and, according to eq. (5), the results should not depend on porosity. Furthermore, all Fontainebleau samples are quartz-pure (i.e. $G_{\text{quartz}} \sim 45 \text{ GPa}$, $\nu_{\text{quartz}} \sim 0.06$, and $\gamma_0 \sim 0.45 \text{ J/m}^2$) and have a constant grain radius (of about $r \sim 100 \mu\text{m}$), whichever the porosity.

The model of Murphy *et al.* (1984) assumes that, for a given rock under fixed room T – P conditions (i.e. $F \sim 0$), elastic weakening solely originates from surface energy γ variations. All the other parameters are constant for the Fontainebleau samples studied. Following this assumption, γ is inverted using a standard least-square [i.e. $LS(\gamma)$] minimization between modelled EWV_{mod} and measured EWV_{mes} elastic wave velocity such that:

$$LS(\gamma) = [EWV_{\text{mod}}(F, G_m, \nu_m, r, \gamma_0, \gamma) - EWV_{\text{mes}}]^2, \quad (6)$$

where EWV stands for either P - or S -wave velocity, and EWV_{mod} is obtained from eqs (2)–(5). Owing to this formulation, the inverted γ values remain lower than the quartz vacuum surface energy γ_0 . The surface energy γ considered here corresponds to an homogenization for all load-bearing grain contacts' surface energy γ_i . The calculated γ can be seen as an average effective surface energy.

As shown by eq. (6), γ values are extracted from either P - or S -wave velocity. The dependence to RH of the inverted γ values (Fig. 8) can thus be directly inferred from the normalized P - and S -wave velocities (Fig. 5). The initial vacuum (i.e. γ_0) and vapour saturating pressure (i.e. γ_f) surface energies from the literature (e.g. Murphy *et al.* 1984) are reported for comparison.

The small error-bars in Fig. 8 emphasize the good fit between P - and S -wave data for all samples, which is consistent with eq. (5). Comparing the inverted γ to the prediction related to Gibb's theory (Adamson 1976; Murphy *et al.* 1984; Parks 1984; Chelidze *et al.* 1996), the overall variation appears to be respected and γ decreases with adsorption. Finally, the most important result here is that γ for higher porosity Fontainebleau samples (i.e. FoSp16 and FoSp18) decreases down to about $\gamma_f \sim 0.12 \text{ J m}^{-2}$. This value corresponds to the measured surface energy at vapour pressure (i.e. $\gamma_f \sim 0.13 \text{ J m}^{-2}$) on a quartz crystal (e.g. Murphy *et al.* 1984). This implies that the model of Murphy *et al.* (1984) describes particularly well the phenomenon for the high porosity (i.e. $\phi \geq 16$ per cent) sandstone samples studied. Yet, for the low poros-

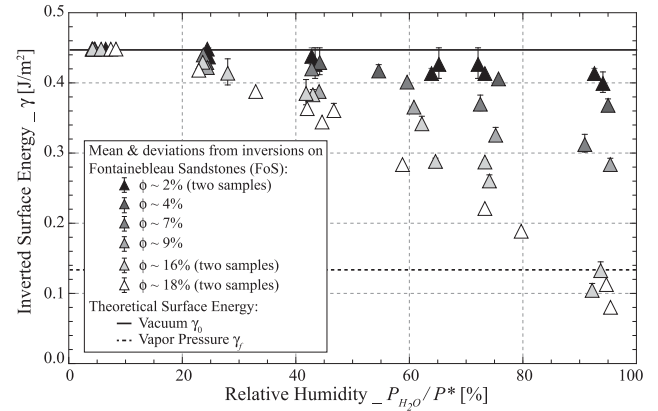


Figure 8. Inverted surface energy using LS minimization between measurements and the model of Murphy *et al.* (1984). Symbols and error bar are, respectively mean and standard deviation obtained from surface energies inverted separately from P - and S -wave measurements and models. Surface energies measured by Parks (1984) on a quartz surface under dry and vapour saturating pressure (P^*) conditions.

ity samples, changes in γ are smaller. This lower dependence of γ points to the fact that the model is less appropriate for these samples.

4.2 Low-porosity sandstone samples: modified model

The above observations suggest that the nature of grain contacts, and their degree of bonding play a role. This is precisely what the model of Digby (1981) takes into account through an additional parameter, namely the bonding radius b .

4.2.1 Model derivation: bonding at a grain contact

As shown in Fig. 6(b), Digby (1981) considered in a mechanistic approach that neighbouring grains are bonded across a circular region of radius b . The applied external force F thus not only depends on a_0 and r as in Hertz's theory, but also on b such that (Digby 1981):

$$F = \frac{4G_m}{3(1 - \nu_m)} \frac{\sqrt{a_2^2 - b^2}}{r} (2a_2^2 + b^2). \quad (7)$$

Note that (i) for $b = 0$ one finds back Hertz–Mindlin's relation between F and $a_2 = a_0$; (ii) in case of no applied force (i.e. $F = 0$), $a_2 = b$ and (iii) under pressure, the contact radius a_0 increases such that $a_2 \geq b$.

Let us now modify the purely mechanistic approach of Digby (1981) to introduce the effect of surface forces (Fig. 6b). Following the approach (eq. 2) of Johnson *et al.* (1971), the total forces F_{tot} at the grain contact may be written in a first approximation as:

$$F_{\text{tot}} = F + F_{\text{surf}} = \left[F + 6\gamma\pi r + \sqrt{12\gamma\pi r F + (6\gamma\pi r)^2} \right]. \quad (8)$$

Introducing surface forces and thus replacing F by F_{tot} in eq. (7), one obtains:

$$\sqrt{a_3^2 - b^2} (2a_3^2 + b^2) = \frac{3(1 - \nu_m)r}{4G_m} [F + 6\gamma\pi r + \sqrt{12\gamma\pi r F + (6\gamma\pi r)^2}], \quad (9)$$

Note that (i) for $F = 0$, one does not find $a_3 = b$ any more, and the relation $a_3 \geq b$ remains true for any external load; (ii) the limiting

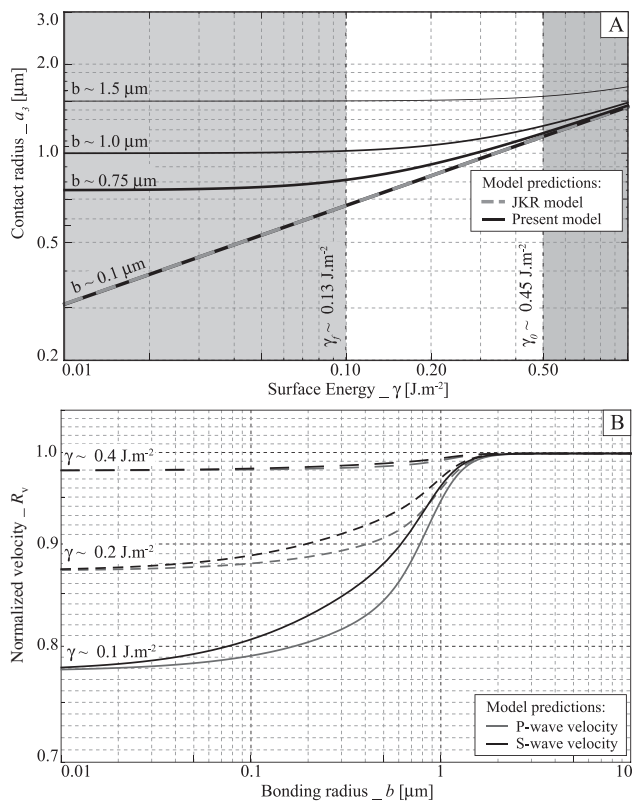


Figure 9. Predictions using the modified model: (a) contact radius a_3 as a function of surface energy γ for different values of bonding radius b (i.e. black lines); (b) normalized P-wave (i.e. black curve) and S-wave (i.e. grey curve) velocities as a function of the bonding radius b for different values of surface energy γ .

case of $a_3 = b$ is observed only if none of the forces exist such that $F_{\text{tot}} = 0$ (i.e. $F = 0$ and $\gamma = 0$) and (iii) eq. (9) remains valid, and surface forces dominate, for low F only.

The new grain contact radius a_3 is then obtained by solving the polynomial equation (eq. 9). The predictions of $a_3 = f(\gamma)$ for differing values of b are compared to the JKR model (eq. 2) in Fig. 9(a). It appears that (i) a_3 falls in the asymptotic values of a_1 (eq. 2) at elevated surface energies and (ii) for $\gamma \in [0.1; 0.5] \text{ J.m}^{-2}$, the dependence of a_3 on γ decreases with increasing b and becomes apparently constant for $b \sim 2 \mu\text{m}$.

The effective compressional (i.e. M_3) and shear (i.e. G_3) moduli of a cemented rock are obtained from this modified model as:

$$\begin{cases} M_3 = \frac{a_3}{r} \frac{G_m(1-\phi)\psi}{5\pi} \left(\frac{3}{1-\nu_m} + \frac{b}{a_3} \frac{4}{2-\nu_m} \right) \\ G_3 = \frac{a_3}{r} \frac{G_m(1-\phi)\psi}{5\pi} \left(\frac{1}{1-\nu_m} + \frac{b}{a_3} \frac{3}{2-\nu_m} \right). \end{cases} \quad (10)$$

By normalizing M_3 (or G_3) by the reference state $M_3(\gamma_0) = M_{30}$ (or $G_3(\gamma_0) = G_{30}$), one obtains:

$$\begin{cases} \frac{M_3}{M_{30}} = \frac{3(2-\nu_m)a_3 + 4b(1-\nu_m)}{3(2-\nu_m)a_{30} + 4b(1-\nu_m)} \\ \frac{G_3}{G_{30}} = \frac{(2-\nu_m)a_3 + 3b(1-\nu_m)}{(2-\nu_m)a_{30} + 3b(1-\nu_m)}, \end{cases} \quad (11)$$

thus implying that:

$$\frac{M_3}{M_{30}} \neq \frac{G_3}{G_{30}} \neq \frac{a_3}{a_{30}}. \quad (12)$$

The normalized P - and S -wave velocities (i.e. RV_p and RV_s) are directly obtained from the normalized compressional (i.e. M_3) and shear (i.e. G_3) moduli, respectively. Their predicted dependence to the bonding radius b is introduced (Fig. 9b) for three different values of γ . Note that the bonding effect becomes negligible for $b \ll 0.1 \mu\text{m}$, and large changes in velocities occur for bonding radius lower than about $b \sim 2 \mu\text{m}$. Above this b value, no change is observed. This rupture point corresponds to the point where bonding forces overcome surface forces. From strength considerations, such critical value is in fact directly inferred from eq. (9). It corresponds to the value for which the bonding strength is much larger than the surface forces:

$$\frac{8G_m b^3}{3(1-\nu_m)r} \gg 12\gamma_0\pi r. \quad (13)$$

For intermediate bonding radius b , a deviation appears between normalized P - (i.e. RV_p) and S -wave (i.e. RV_s) velocities (Fig. 9b). This deviation decreases at higher bonding values up to $b \sim 2 \mu\text{m}$ where $RV_p \sim RV_s \sim 1$.

4.2.2 Estimation of the surface energy

Using the modified model, surface energy is again inverted using a similar least-square minimization as detailed in eq. (6). Again, the parameters relate to a quartz-pure rock (i.e. $G_{\text{quartz}} \sim 45 \text{ GPa}$, $\nu_{\text{quartz}} \sim 0.06$, and $\gamma_0 \sim 0.45 \text{ J.m}^{-2}$) with a given grain radius (i.e. $r \sim 100 \mu\text{m}$) under atmospheric conditions (i.e. $F \sim 0 \text{ N}$). The modified model (eq. 11) introduces the bonding radius b as an additional parameter. For the inversion, the parameter b is fixed so that $\gamma \sim 0.13 \text{ J.m}^{-2}$ is obtained for the highest value of RH.

The resulting surface energies, along with the values of b (and related ratio b/a_3) used, are reported (Fig. 10) as a function of the samples' porosity. Such procedure leads to inverted surface energy values for all samples falling in the same overall trend (Fig. 10a) that was found using the model of Murphy *et al.* (1984) on the most porous samples (Fig. 8).

Note that a scattering appears between P and S waves inverted γ values for low porosity samples (Fig. 10a). This effect probably results from the small variations measured in low porosity samples. From the reported table (Fig. 10b), it appears that one can find realistic values of b . Yet, values found for all samples with porosities lower than about ~ 9 per cent fall in a very narrow range of about $b \sim 0.5\text{--}1.5 \mu\text{m}$.

5 DISCUSSION

The presented results and interpretations raise several questions on three issues: (i) the relation between bonding radius b and porosity; (ii) the relation between elastic weakening and saturation and (iii) the effect of RH on attenuation.

5.1 Relation between bonding radius and porosity

To complement the present data set on Fontainebleau samples, another data set from Gomez *et al.* (2010) is useful. It corresponds to measurements of elastic wave velocities at higher confining pressures (i.e. $P_c \sim 40 \text{ MPa}$). The porosity dependence of the Fontainebleau samples' elastic properties measured at room P conditions and at 40 MPa are compared (Fig. 11). As shown by the P - and S -wave velocity zones, the pressure effect increases with porosity.

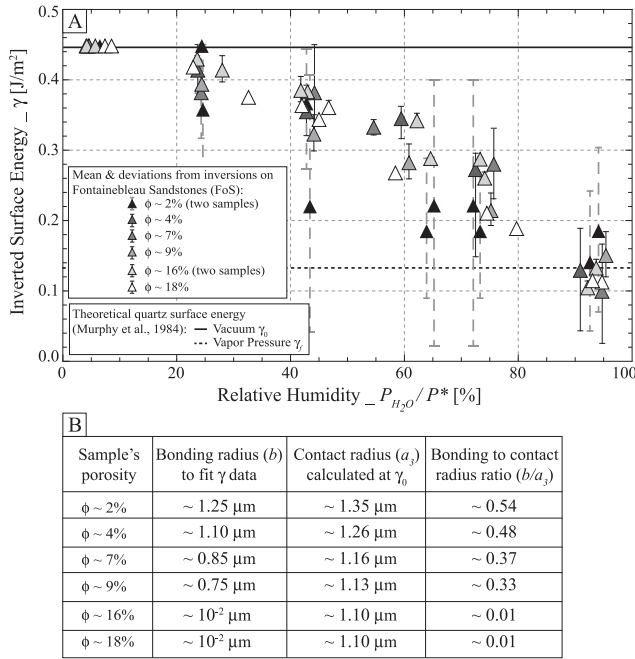


Figure 10. Data obtained using the modified model: (a) inverted surface energy using LS minimization between measurements and the modified model. Symbols and error bar are respectively mean and standard deviation obtained from surface energies inverted separately from P - and S -wave measurements and models; (b) values of bonding radius allowing for consistent surface energy values at higher RH, and grain contact radius calculated (eq. 9) under dry conditions (γ_0).

The measured P - and S -wave velocities at room P-T are then normalized over high confining measurements from Gomez *et al.* (2010). The variations of normalized RV_p and RV_s with porosity are reported (Fig. 12a). It appears that normalized velocities show a clear decrease with increasing porosity, and both RV_p and RV_s show very similar dependence to porosity. This decrease can be related to the degree of cement of a given Fontainebleau sample. Such a result could be understood as a variation of the ratio b/a_3 in porous sandstones. In the same manner, one may predict the effect of confining pressure on the effective moduli by determining the change in contact radius a_3 using the model (eq. 10) of Digby (1981). Assuming a value of $a' \gg b$ at high confining pressure (i.e. $P_c \sim 40 \text{ MPa}$), and normalizing the dry elastic moduli at room T-P (i.e. M_{30}) by the high confining state (i.e. M') one obtains:

$$\begin{cases} \frac{M_{30}}{M'} \sim \frac{a_{30}}{a'} \left(1 + \frac{4}{3} \frac{b}{a_{30}} \frac{1 - \nu_m}{2 - \nu_m} \right) \\ \frac{G_{30}}{G'} \sim \frac{a_{30}}{a'} \left(1 + 3 \frac{b}{a_{30}} \frac{1 - \nu_m}{2 - \nu_m} \right), \end{cases} \quad (14)$$

From the experimental conditions, a' and a_{30} differ from the applied external load (i.e. F_{\max} and F_{atm} , respectively). Assuming here the surface energy equal to $\gamma_0 \sim 0.45 \text{ J m}^{-2}$ for the data set, both a' and a_{30} can directly be inferred from eq. (9) as a sole function of the variable b such that:

$$\begin{cases} a_{30}(b) = a_3(G_{\text{qtz}}, \nu_{\text{qtz}}, r, F_{\text{atm}}, \gamma_0, b) \\ a'(b) = a_3(G_{\text{qtz}}, \nu_{\text{qtz}}, r, F_{\max}, \gamma_0, b), \end{cases} \quad (15)$$

Noting that $F \sim Pr^2$, F_{\max} and F_{atm} are expected to differ by about two orders of magnitude. We choose $F_{\max} \sim 1 \text{ N}$ for the measurements at high confining pressure

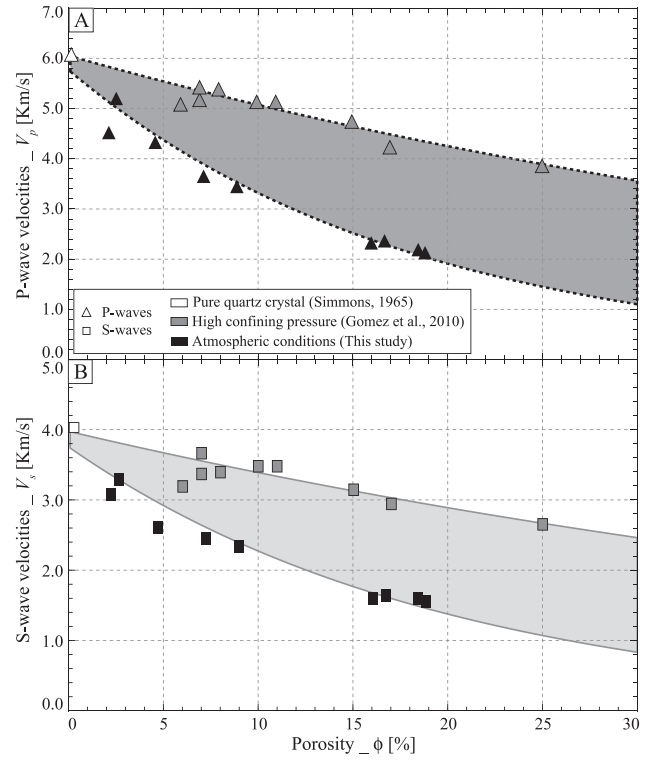


Figure 11. Dependence of elastic wave velocities to porosity for Fontainebleau sandstones between measurements at lowest relative humidity and ambient conditions (black symbols), and data set from Gomez *et al.* (2010) measured at elevated (i.e. $P_c \sim 40 \text{ MPa}$) confining pressure (grey symbols). The grey areas (i.e. dark-grey for P waves and light-grey for S waves) between the best-fitting trend-lines represent the effect of pressure on load bearing grain contacts.

(i.e. $P_c \sim 40 \text{ MPa}$) and $F_{\text{atm}} \sim 10^{-2} \text{ N}$ for the ones at atmospheric conditions. Finally, the other parameters being fixed, the ratio defined from eq. (14) are a sole function of the bonding radius b . To invert for b , as in eq. (6), a least-square minimization is then applied to the difference between the normalized model (eq. 10) and data (Fig. 12a).

The values of bonding radius b obtained with this method are compared (Fig. 12b) to the ones obtained in Section 4 (Fig. 10b). It appears from Fig. 12(b) that both methods lead to relatively similar values of bonding radius b . While the values found from eq. (14) overestimate the ones from eq. (10), the overall trend seems to be respected and the b values decrease with increasing porosity. The deviation found could originate from the different hypothesis made, but the modified model introduced in Section 4.2 (eq. 9) seems to qualitatively account for adsorption on cemented granular rocks.

5.2 Relation between saturation and elastic weakening

While adsorption (and thus S_w) remains the limiting factor without which no elastic weakening would be observed, it was shown in Section 3 that elastic weakening (Fig. 5) and S_w (Fig. 3) from adsorption do not correlate. In particular, the absence of weakening in any of the 11 limestones rises a question. Is the absence of weakening in limestones related to its non-granular microstructure or to an intrinsic difference between calcite and quartz?

Saturation from RH relies on physisorption of water molecules on the mineral surfaces, which relates to (i) affinity of a mineral to water (e.g. Maghsoudy-Louyeh & Tittmann 2008) and (ii) the

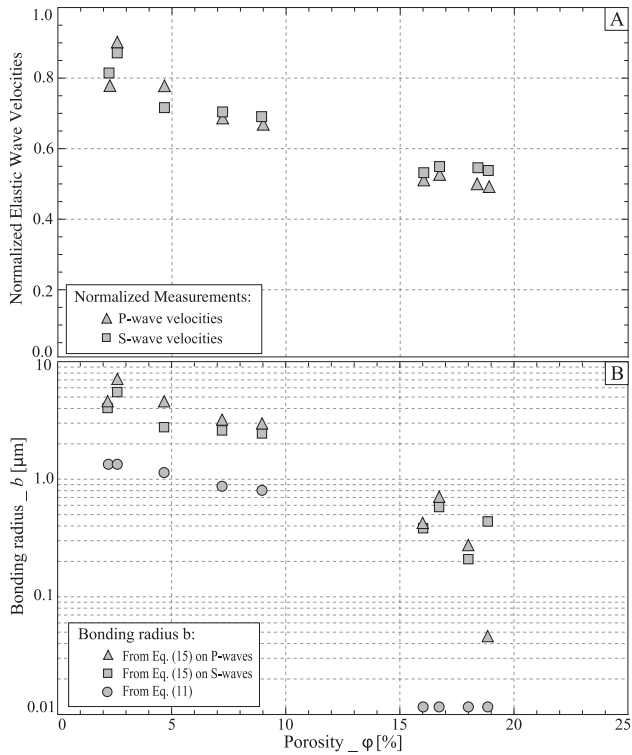


Figure 12. (a) P - and S -wave velocities (i.e. grey triangles and squares, respectively) measured at ambient conditions normalized as a function of high confining measurements from Gomez *et al.* (2010) plotted against porosity. b) Comparison of the bonding radius b obtained using either results from the adsorption study (i.e. light-grey dots) or the confining study for P -wave (i.e. light-grey triangles) and S -wave (i.e. light-grey squares) measurements.

amount of surface allowing for adsorption (e.g. Goertz & Knight 1998). Quartz crystals are known to bear a large affinity to water, leading to large quantities (up to several monolayers) of adsorption on the mineral surface (e.g. Goertz & Knight 1998). Measurements by Maghsoudy-Louyeh & Tittmann (2008) showed that adhesion forces on quartz, mica and calcite minerals (i) are of the same magnitude and (ii) increase similarly with RH. It may indicate that affinity of both minerals to adsorbed water is of the same order of magnitude, and implies that the measured differences in saturation between limestones and sandstones do not relate here to a difference in mineral affinity.

The water saturation S_w is the measure of mass change (Δm) from adsorption over the pore volume (V_{pore}). As mass changes occur solely from adsorption on the pore surface, S_w can also be written as a function of the number of moles of water (α) adsorbed on the internal surface (S_{pore}) such that:

$$S_w = \alpha \cdot \frac{S_{\text{pore}}}{\rho_{\text{wat}} \cdot V_{\text{pore}}} \quad (16)$$

The fact that S_w varies very weakly with porosity in Fontainebleau samples indicates that the specific surface area (S_s) weakly depends on porosity, which is consistent with Bourbie & Zinszner (1985). The large differences in S_w between Fontainebleau sandstone and limestone samples is probably linked to differences in specific surface area. As an example, Dana & Skoczyłas (1999) measured a very low specific surface area (i.e. $S_{s\text{FoS}} \sim 0.03 \text{ m}^2 \text{ g}^{-1}$) on a Fontainebleau sample of $\phi \sim 9$ per cent porosity. On the opposite, large specific surface areas ranging up to about $S_{s\text{LS}} \sim 3 \text{ m}^2 \text{ g}^{-1}$ were measured by Vincent *et al.* (2011) on some microporous lime-

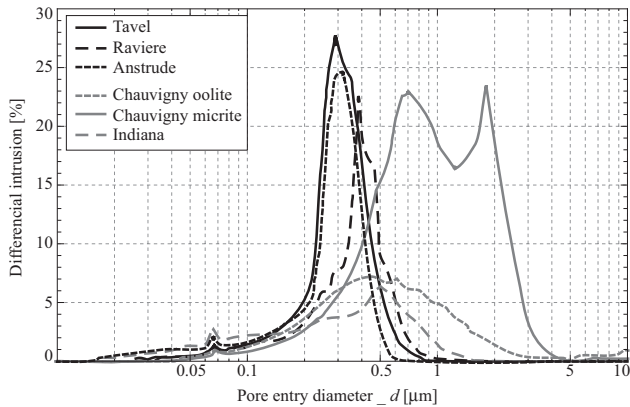


Figure 13. Normalized intruded volume as a function of pore entry diameter measured using a typical MICP technique. Example of measurements for six representative limestone samples.

stone samples, and by Clark *et al.* (1980) on their limestones and sandstones samples. This may explain the large differences in saturation between Fontainebleau sandstone and the rocks measured by Clark *et al.* (1980).

Note that the largest S_w (at high RH) are obtained for the Anstrude, Raviere, Massangis and Tavel limestones. A standard procedure of mercury injection (i.e. MICP) was used to study these rocks' pore entry diameters (e.g. Casteleyn *et al.* 2010). On the contrary to other limestones, MICP measurements (Fig. 13) on three of these four rocks show a narrow peak for very small pore entry diameters of sub-microns size. MICP measurements may thus confirm that adsorption relates to pores size, and thus to specific surface area.

5.3 Waves amplitudes variations and attenuation

As observed from Fig. 4, the waveform's amplitude is also affected by RH. As for elastic waves velocities, P - and S -waves amplitudes show large decrease with increasing RH in the Fontainebleau sample studied (Fig. 4b). To characterize this effect, the Fourier spectra of the full waveforms can be directly computed, as shown for the example of P -amplitude spectra (Fig. 14) of the two samples chosen (Fig. 4). Again, a clear difference is observed between the limestone (Fig. 14a) and FoSp16a (Fig. 14b) P -amplitudes spectra. While the limestone spectra show no change with RH, large decrease in P amplitude is observed for FoSp16a with increasing RH. In particular, the normalized amplitude obtained for FoSp16 between measurements under dry (i.e. A_0) and maximum RH conditions (i.e. A_i) is as low as about $A_i/A_0 \sim 0.2$.

Waves attenuations, in terms of quality factors, could be obtained using the spectrum ratio principle (Toksoz *et al.* 1976; Bourbie & Zinszner 1985) from these amplitude variations. Assuming that attenuation relates to amplitude variations would lead to the conclusion that elastic weakening and attenuation correlate in their RH dependence. Such result, of elastic weakening and attenuation variations with RH, was observed by Clark *et al.* (1980). As assumed by different authors (e.g. Murphy *et al.* 1986; Chelidze *et al.* 1996), dispersion and attenuation from moisture are thought to originate from fluid movements at the grain contacts, and could be expected to occur in granular rocks. Yet, reporting such measurement would imply (i) using as a reference the amplitude of a non-attenuating standard such as an aluminium (e.g. Bourbie & Zinszner 1985) and (ii) compare the amplitudes of the different samples, which

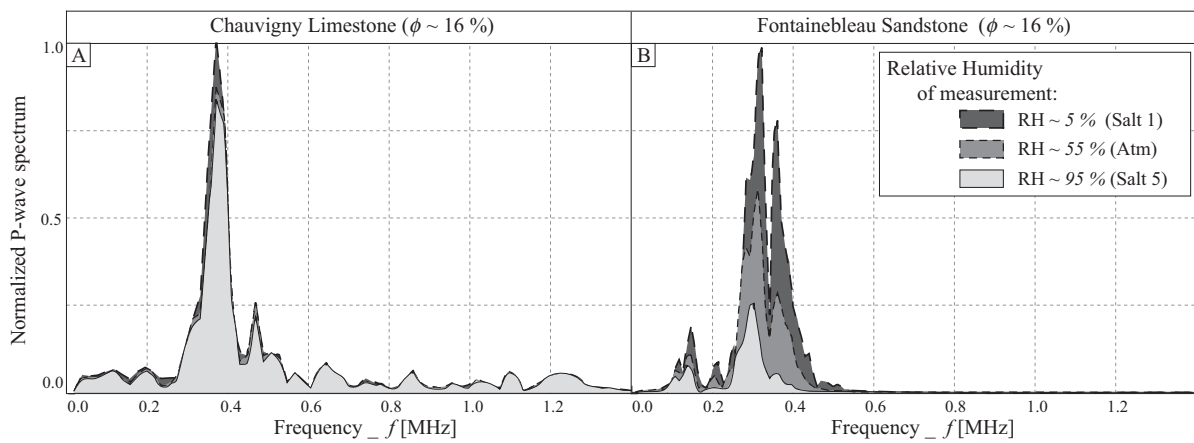


Figure 14. Normalized P -wave Fourier spectra measured at ambient conditions on a Chauvigny limestone and a Fontainebleau sandstone sample for three different Relative Humidities.

is obtained with different contact positions and quality. As a consequence, attenuation was not investigated here to concentrate on elastic weakening.

Note that, previously, elastic weakening (Clark *et al.* 1980) and attenuation (e.g. Tittmann 1977, 1978; Clark *et al.* 1980; Tittmann *et al.* 1980) from adsorption have only been measured at lower frequencies (i.e. $f \sim 1$ kHz). In the particular case of measurements by Clark *et al.* (1980), elastic properties are obtained using the Resonant Bar Technique (e.g. Tittmann *et al.* 1980). This widely used apparatus allows for measurements of shear and extensional elastic moduli and seismic attenuation at intermediate frequencies (i.e. $f \in [1; 20]$ kHz). On the reverse, the present data set was obtained using a typical ultrasonic apparatus leading to waves frequency of about $f \sim 0.3$ MHz. This experiment thus complements existing data sets and shows that, at a given RH, attenuation and elastic weakening also appear at frequencies as high as $f \sim 0.3$ MHz.

5.4 Surface energy variations from adsorption

As shown above, a variation in surface energy (γ) with increasing RH (Figs 8 and 10) is inferred. In particular, the values obtained (at high RH) using the model of Murphy *et al.* (1984) in the case of the most porous sandstones (Fig. 8) fit particularly well the value of $\gamma_f \sim 0.13$ J m⁻² directly measured at vapour saturating pressure on a quartz surface by Parks (1984). Furthermore, using the newly developed model, the same γ value can be reached for all Fontainebleau samples for realistic values of bonding radii b .

Using BET theory (Adamson 1976), Murphy *et al.* (1984) predicted the RH dependence of γ . As schematized by Parks (1984), the prediction is that γ variations are much larger at the lowest RH. The first adsorbed monolayer is expected to develop at very low RH values (i.e. ~ 10 per cent), and to strongly affect γ . This strong effect at low RH values is not supported by the estimates for surface energy values inferred from the measurements on Fontainebleau sandstone's samples (Figs 8 and 10). While investigating the cause for such deviation may be of interest, it would imply modelling the thermodynamics of adsorption variations at an interface and its effect on surface energy. Such investigation is out of the scope of this study.

6 CONCLUSIONS

An experimental set-up has been designed to investigate the effect of adsorption on limestones and sandstone samples' elastic properties.

From varying RH, saturation and elasticity measurements at ultrasonic frequencies (i.e. $f \sim 0.5$ MHz) on limestones and sandstones have been obtained. The results show that RH affects the sample properties. Both rock types show varying degrees of adsorption with RH, and varying effects on elasticity. Limestones show large adsorption effects, but no elastic weakening is observed. On the reverse, large elastic weakening is observed on Fontainebleau sandstone samples. The weakening effects measured are similar for P - and S -wave velocities.

As elastic weakening affects preferentially the granular sandstones, grain contact theories have been used to interpret the present measurements. Using the model of Murphy *et al.* (1984), the rock-fluid adsorption effect is explained in terms of surface energy variations (Johnson *et al.* 1971; Murphy *et al.* 1984). It appears that this model predicts the same weakening for both P - and S -wave velocities, which is consistent with the data. An effective surface energy is obtained for the Fontainebleau samples. For the highest porosity samples, this surface energy proves to be consistent with quartz mineral surface energy at vapour saturating pressure. The model of Murphy *et al.* (1984) describes well high porosity loosely cemented sandstones.

Yet, the amount of variation in surface energy with RH decreases with decreasing the sample porosity and a very small variation is found for the lowest porosity sandstones. Fontainebleau sandstone is a typical granular rock in which cementation increases with decreasing porosity. In order to account for this, the approach of Murphy *et al.* (1984) has been modified using the cemented granular model of Digby (1981). An additional parameter is the bonding radius b . For the problem's parameters at hand, it was found that surface effects are important only for values of b lower than about $b \sim 2$ μ m.

In addition, a comparison between limestones and sandstones shows that the fundamental difference between their respective elastic weakening from adsorption originate from a microstructural difference. Fontainebleau sandstone is a typical grain aggregate where the contact between grains is a key parameter. On the reverse, limestones may be considered as bearing porosity embedded in a very fine cemented matrix.

ACKNOWLEDGEMENTS

The authors would like to thank Prof Christian David from the University of Cergy and Dr Elizabeth Bemer from IFPEN for providing us with limestones samples. Prof Christian David and Jean-Christian

Coulombier are thanked for their help on MICP measurements on some of the samples.

REFERENCES

Adam, L., Batzle, M. & Brevik, I., 2006. Gassmann's fluid substitution and shear modulus variability in carbonates at laboratory seismic and ultrasonic frequencies, *Geophysics*, **71**(6), F173–F183.

Adamson, A.W., 1976. *Physical Chemistry of Surfaces*, 2nd edn, Wiley.

Assefa, S., McCann, C. & Sothcott, J., 2003. Velocities of compressional and shear waves in limestones, *Geophys. Prospect.*, **51**(1), 1–13.

Baechle, G.T., Weger, R.J., Eberli, G.P., Massaferro, J.L. & Sun, Y.F., 2005. Changes of shear moduli in carbonate rocks implications for Gassmann applicability, *Leading Edge*, **24**(5), 507–510.

Baud, P., Zhu, W. & Wong, T.-f., 2000. Failure mode and weakening effect of water on sandstone, *J. geophys. Res.: Solid Earth (1978–2012)*, **105**(B7), 16 371–16 389.

Bourbie, T. & Zinszner, B., 1985. Hydraulic and acoustic properties as a function of porosity in Fontainebleau sandstone, *J. geophys. Res.: Solid Earth (1978–2012)*, **90**(B13), 11 524–11 532.

Casteleyn, L. *et al.*, 2010. Interrelations of the petrophysical, sedimentological and microstructural properties of the oolithe blanche formation (bathonian, saline aquifer of the Paris basin), *Sediment. Geol.*, **230**(3–4), 123–138.

Chelidze, T.L., Spetzler, H.A. & Sobolev, G.A., 1996. Absorption of strain waves in porous media at seismic frequencies, *Pure appl. Geophys.*, **147**(1), 25–55.

Clark, V.A., Tittmann, B.R. & Spencer, T.W., 1980. Effect of volatiles on attenuation (q -1) and velocity in sedimentary rocks, *J. geophys. Res.: Solid Earth (1978–2012)*, **85**(B10), 5190–5198.

Dana, E. & Skoczyłas, F., 1999. Gas relative permeability and pore structure of sandstones, *Int. J. Rock Mech. Min. Sci.*, **36**(5), 613–625.

Digby, P.J., 1981. The effective elastic moduli of porous granular rocks, *J. appl. Mech.*, **48**, 803–808.

Duda, M. & Renner, J., 2013. The weakening effect of water on the brittle failure strength of sandstone, *Geophys. J. Int.*, **192**(3), 1091–1108.

Eslami, J., Grgic, D. & Hoxha, D., 2010. Estimation of the damage of a porous limestone from continuous (P- and S-) wave velocity measurements under uniaxial loading and different hydrous conditions, *Geophys. J. Int.*, **183**(3), 1362–1375.

Fabricius, I.L., Bächle, G.T. & Eberli, G.P., 2010. Elastic moduli of dry and water-saturated carbonates—effect of depositional texture, porosity, and permeability, *Geophysics*, **75**(3), N65–N78.

Fortin, J., Guéguen, Y. & Schubnel, A., 2007. Effects of pore collapse and grain crushing on ultrasonic velocities and V_p/V_s , *J. geophys. Res.: Solid Earth (1978–2012)*, **112**(B8), B08207, doi:10.1029/2005JB004005.

Fortin, J., Stanchits, S., Dresen, G. & Guéguen, Y., 2009. Micro-mechanisms involved during inelastic deformation of porous carbonate rocks, in *Poro-Mechanics IV*, pp. 378–383, eds Ling, H.I., Smyth, A. & Betti, R., DEStech Publications.

Gassmann, F., 1951. Elasticity of porous media, *Vierteljahrsschrift der Naturforschenden Gesellschaft*, **96**, 1–23.

Goertz, D. & Knight, R.J., 1998. Elastic wave velocities during evaporative drying, *Geophysics*, **63**(1), 171–183.

Gomez, C.T., Dvorkin, J. & Vanorio, T., 2010. Laboratory measurements of porosity, permeability, resistivity, and velocity on Fontainebleau sandstones, *Geophysics*, **75**(6), E191–E204.

Greenspan, L., 1977. Humidity fixed points of binary saturated aqueous solutions, *J. Res. Natl. Bureau Stand., A. Phys. Chem.*, **81**, 89–96.

Johnson, K.L., Kendall, K. & Roberts, A.D., 1971. Surface energy and the contact of elastic solids, *Proc. R. Soc. Lond. A, Math. Phys. Sci.*, **324**(1558), 301–313.

Kirby, S.H., 1984. Introduction and digest to the special issue on chemical effects of water on the deformation and strengths of rocks, *J. geophys. Res.*, **89**(B6), 3991–3995.

Klein, E., Baud, P., Reuschlé, T. & Wong, T.F., 2001. Mechanical behaviour and failure mode of bentheim sandstone under triaxial compression, *Phys. Chem. Earth, Part A: Solid Earth Geod.*, **26**(1), 21–25.

Le Guen, Y., Renard, F., Hellmann, R., Brosse, E., Collombet, M., Tisserand, D. & Gratier, J.-P., 2007. Enhanced deformation of limestone and sandstone in the presence of high $p\text{CO}_2$ fluids, *J. geophys. Res.*, **112**(B5), B05421, doi:10.1029/2006JB004637.

Maghsoudy-Louyeh, S. & Tittmann, B.R., 2008. Assessment of hydrous affinity of selected material, *Coll. Surf. A: Physicochem. Eng. Aspects*, **331**(3), 268–274.

Mindlin, R.D., 1949. Compliance of elastic bodies in contact, *J. appl. Mech.*, **16**, 353–383.

Murphy, W.F. III, 1982. Effects of partial water saturation on attenuation in Massilon sandstone and Vycor porous glass, *J. acoust. Soc. Am.*, **71**, 1458–1468.

Murphy, W.F., 1984. Acoustic measures of partial gas saturation in tight sandstones, *J. geophys. Res.: Solid Earth (1978–2012)*, **89**(B13), 11 549–11 559.

Murphy, W.F., Winkler, K.W. & Kleinberg, R.L., 1984. Frame modulus reduction in sedimentary rocks: the effect of adsorption on grain contacts, *Geophys. Res. Lett.*, **11**(9), 805–808.

Murphy, W.F., Winkler, K.W. & Kleinberg, R.L., 1986. Acoustic relaxation in sedimentary rocks: dependence on grain contacts and fluid saturation, *Geophysics*, **51**(3), 757–766.

Ougier-Simonin, A., Fortin, J., Guéguen, Y., Schubnel, A. & Bouyer, F., 2011. Cracks in glass under triaxial conditions, *Int. J. Eng. Sci.*, **49**(1), 105–121.

Pandit, B.I. & King, M.S., 1979. The variation of elastic wave velocities and quality factor q of a sandstone with moisture content, *Can. J. Earth Sci.*, **16**(12), 2187–2195.

Parks, G.A., 1984. Surface and interfacial free energies of quartz, *J. geophys. Res.: Solid Earth (1978–2012)*, **89**(B6), 3997–4008.

Song, I. & Renner, J., 2008. Hydromechanical properties of Fontainebleau sandstone: experimental determination and micromechanical modeling, *J. geophys. Res.*, **113**(B9), B09211, doi:10.1029/2007JB005055.

Sulem, J. & Ouffroukh, H., 2006. Hydromechanical behaviour of Fontainebleau sandstone, *Rock Mech. Rock Eng.*, **39**(3), 185–213.

Tittmann, B.R., 1977. Lunar rock q in 3000–5000 range achieved in laboratory, *Phil. Trans. R. Soc. Lond., A, Math. Phys. Sci.*, **285**(1327), 475–479.

Tittmann, B.R., 1978. Internal friction measurements and their implications in seismic q structure models of the crust, *Geophys. Monogr. Ser.*, **20**, 197–213.

Tittmann, B.R. & Housley, R.M., 1973. High q (low internal friction) observed in a strongly outgassed terrestrial analog of lunar basalt, *Phys. Status Solidi (b)*, **56**(2), K109–K111.

Tittmann, B.R., Clark, V.A., Richardson, J.M. & Spencer, T.W., 1980. Possible mechanism for seismic attenuation in rocks containing small amounts of volatiles, *J. Geophys. Res.: Solid Earth (1978–2012)*, **85**(B10), 5199–5208.

Toksöz, M.N., Cheng, C.H. & Timur, A., 1976. Velocities of seismic waves in porous rocks, *Geophysics*, **41**(4), 621–645.

Tutuncu, A.N. & Sharma, M.M., 1992. The influence of fluids on grain contact stiffness and frame moduli in sedimentary rocks, *Geophysics*, **57**(12), 1571–1582.

Vajdova, V., Baud, P. & Wong, T., 2004. Compaction, dilatancy, and failure in porous carbonate rocks, *J. geophys. Res.*, **109**(B5), B05204, doi:10.1029/2003JB002508.

Vajdova, V., Zhu, W., Natalie Chen, T.M. & Wong, T., 2010. Micromechanics of brittle faulting and cataclastic flow in tavel limestone, *J. Struct. Geol.*, **32**(8), 1158–1169.

Verwer, K., Braaksma, H. & Kenter, J.A.M., 2008. Acoustic properties of carbonates: effects of rock texture and implications for fluid substitution, *Geophysics*, **73**(2), B51–B65.

Vincent, B., Fleury, M., Santerre, Y. & Brigaud, B., 2011. Nmr relaxation of neritic carbonates: an integrated petrophysical and petrographical approach, *J. appl. Geophys.*, **74**(1), 38–58.

Wang, Z. & Nur, A., 1992. Elastic wave velocities in porous media: a theoretical recipe, *Seism. acoust. Velocit. Reservoir Rocks*, **2**, 1–35.

Winkler, K.W. & Murphy, W.F. III, 1995. Acoustic velocity and attenuation in porous rocks, in *Rock Physics and Phase Relations, A Handbook of Physical Constants*, AGU Reference Shelf 3, American Geophysical Union.

Youssef, S., Han, M., Bauer, D., Rosenberg, E., Bekri, S., Fleury, M. & Vizika, O., 2008. High resolution μ cct combined to numerical models to assess electrical properties of bimodal carbonates, in *Proceedings of the 22nd International Symposium of the Society of Core Analysts*, Abu Dhabi, UAE.